Received: 8 October 2022 | Accepted: 19 December 2022

DOI: 10.1002/pamm.202200246

Application of a microplane damage model for concrete to an isogeometric scaled boundary formulation for 3D solids

Georgia Kikis[1,*], **Leonie Mester**[1], **Rostislav Chudoba**[2], and **Sven Klinkel**[1]

[1] Lehrstuhl für Baustatik und Baudynamik, RWTH Aachen, Mies-van-der-Rohe-Str. 1, 52074 Aachen, Germany
[2] Lehrstuhl und Institut für Massivbau, RWTH Aachen, Mies-van-der-Rohe-Str. 1, 52074 Aachen, Germany

Microplane models have the advantage of describing damage-induced anisotropy, which is common in quasi-brittle materials such as concrete, in a simple and straightforward way. Over the past decades, various microplane models have been formulated to describe different loading cases and phenomena in concrete structures. They include pure damage and pure plasticity based microplane models or a combination of these two approaches. In this work, as a first step, a microplane damage model, which is derived from the principle of energy equivalence, is applied in the framework of an isogeometric 3D solid in boundary representation. Isogeometric analysis has the advantage that it can represent exactly complex geometries, which can influence the correct description of damage evolution. In addition, the use of a boundary representation in combination with NURBS and B-splines is in accordance with the modeling technique common in CAD and allows for a straightforward application of the design model to the analysis process. The boundary is described using bi-variate NURBS while the interior of the solid is approximated using uni-variate B-splines. The combination of isogeometric analysis with a model that can capture the finely distributed cracking of the concrete matrix represents a modeling strategy that can effectively support the development of thin-walled shell structures made of textile-reinforced concrete. Several examples are studied in order to investigate the ability of the microplane damage model to correctly describe quasi-brittle fracture in this kind of non-standard discretization formulation. Furthermore, a comparison to the standard finite element method is conducted.

1 Scaled Boundary Isogeometric Analysis (SBIGA)

The scaled boundary representation was combined with the isogeometric analysis to describe 3D solids in [1]. The displacements on the boundary are approximated using NURBS basis functions, while in the interior B-splines are used. The solid is described by its boundary surfaces which are scaled along a scaling direction into the scaling center. This way, the solid is divided into sections, where each section consists of a boundary surface that is being scaled. An example of such solids is shown in Fig. 1, where a concrete cube with part of a reinforcement is depicted. The reinforcement and the concrete are then described separately using the scaled boundary representation technique. This is in accordance with the boundary representation modeling technique used in CAD tools. In addition, the use of isogeometric analysis allows for the exact description of complex geometries. The discretized weak form of equilibrium in the case of SBIGA is given as follows

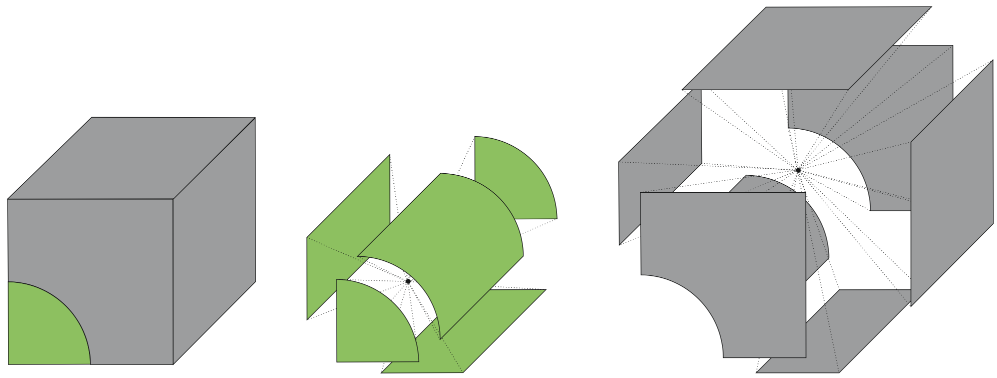

Fig. 1: The SBIGA concept presented for a reinforced concrete cube. In the middle and at the right the "exploded view" of the reinforcement and concrete geometries are shown in accordance to the scaled boundary concept.

$$G(\boldsymbol{u}, \delta\boldsymbol{u}) = \sum_{s=1}^{n_{sec}} \delta\boldsymbol{U}^T \left(\int_{\Omega_{0,s}} \boldsymbol{B}^T \hat{\boldsymbol{F}}^T \boldsymbol{S} \, \mathrm{d}V - \int_{\Omega_{0,s}} \boldsymbol{N}^T \boldsymbol{b}_0 \, \mathrm{d}V - \int_{\partial_t \Omega_{0,s}} \boldsymbol{N}^T \bar{\boldsymbol{t}}_0 \, \mathrm{d}A \right) \tag{1}$$

where n_{sec} is the number of sections, $\Omega_{0,s}$ is the volume of section s, $\boldsymbol{b}_0$ is the body force and $\bar{\boldsymbol{t}}_0$ the boundary traction. The matrix $\hat{\boldsymbol{F}}$, which has the dimension 6×9 includes the components of the deformation gradient, see [1]. The vector $\delta\boldsymbol{U}$

* Corresponding author: kikis@lbb.rwth-aachen.de, phone +49 241 80 25721, fax +49 241 80 22303

includes the nodal degrees of freedom of a section in the scaling direction. $\boldsymbol{S}$ denotes the second Piola-Kirchhoff stress, which is represented in Voigt notation. The basis functions $\boldsymbol{N} = \boldsymbol{N}_b(\eta,\zeta)\boldsymbol{N}_s(\xi)$ depend on $\boldsymbol{N}_b(\eta,\zeta)$ that includes the NURBS basis functions of the boundary surfaces and $\boldsymbol{N}_s(\xi)$ that contains the uni-variate B-spline basis functions in scaling direction. The matrix $\boldsymbol{B}$ is defined as follows

$$\boldsymbol{B} = \frac{1}{\bar{\boldsymbol{J}}}\left(\boldsymbol{b}_1\boldsymbol{N}_b\boldsymbol{N}_{s,\xi} + \frac{1}{\xi}(\boldsymbol{b}_2\boldsymbol{N}_{b,\eta}\boldsymbol{N}_s + \boldsymbol{b}_3\boldsymbol{N}_{b,\zeta}\boldsymbol{N}_s)\right) \tag{2}$$

where $\bar{\boldsymbol{J}}$ is the part of the Jacobian matrix that only depends on the boundary parameters η and ζ. The definition of the matrices $\boldsymbol{b}_1$, $\boldsymbol{b}_2$ and $\boldsymbol{b}_3$ that also depend only on η and ζ can be found in [1].

It should be noted that even though the formulation here is expressed using the second Piola-Kirchhoff stress, and by this extend the Green-Lagrange strains, in the following examples only small strains were considered and $\boldsymbol{S}$ is replaced by $\boldsymbol{\sigma}$.

2 Microplane Damage Model

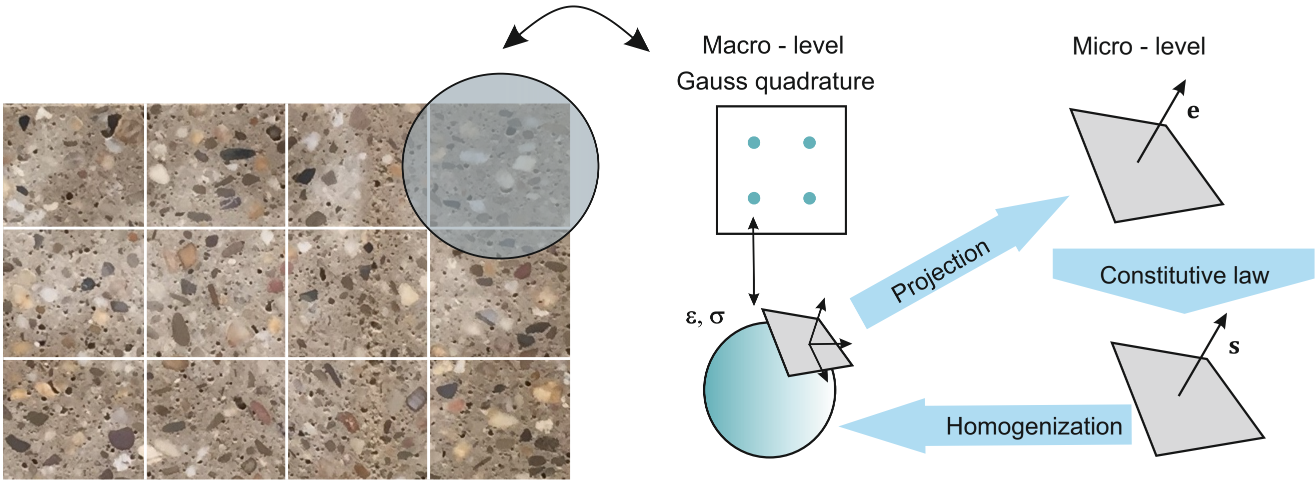

Fig. 2: General procedure when using microplane models.

Microplane models have successfully been applied for modeling concrete and are able to capture its different response for different stress states, as well as naturally describe damage-induced anisotropy, which is common in quasi-brittle materials such as concrete. The general procedure for microplane models includes the projection of the strain tensor at each Gauss point on the so-called microplanes which have different orientations that approximate a sphere (42 in total, when considering symmetry 21). This way, on each microplane a strain vector is defined. The constitutive laws are introduced on the microplane level and the resulting stress vectors are homogenized in order to get the stress tensor, see Fig. 2. The microplane model that is going to be used here is the microplane damage model from Jirásek [2] that has already been successfully applied to thin-walled textile-reinforced concrete shells in [3]. It is based on the principle of energy equivalence, which means that the complementary energy of the damaged material expressed by the apparent stress $\boldsymbol{\sigma}$ is equal to the complementary energy of the undamaged material expressed by the effective stress $\tilde{\boldsymbol{\sigma}}$. The principle of energy equivalence leads to the following definition of the damaged material tensor

$$\boldsymbol{D} = \boldsymbol{\beta} : \boldsymbol{D}^e : \boldsymbol{\beta}^T \tag{3}$$

where $\boldsymbol{\beta}$ is a fourth order damage tensor. The entries of the damaged material tensor $\boldsymbol{D}$ can be expressed as

$$D_{ijkl} = D^e_{pqrs}\beta_{ijpq}\beta_{klrs} = \frac{1}{4}(D^e_{mjnl}\phi_{im}\phi_{kn} + D^e_{imnl}\phi_{jm}\phi_{kn} + D^e_{mjkn}\phi_{im}\phi_{ln} + D^e_{imkn}\phi_{jm}\phi_{ln}). \tag{4}$$

$\boldsymbol{\phi}$ is a symmetric second-order tensor that can be interpreted as the damage from the macroscopic point of view

$$\boldsymbol{\phi} = \frac{3}{2\pi}\int_\Omega \phi\,\boldsymbol{n}\otimes\boldsymbol{n}\,\mathrm{d}\Omega \approx 6\sum_{\mu}^{N_\mu} w_\mu \phi^{(\mu)}\boldsymbol{n}^{(\mu)}\otimes\boldsymbol{n}^{(\mu)} \tag{5}$$

where N_μ is the number of microplanes, w_μ is the weight of each microplane μ and $\boldsymbol{n}$ is the unit normal to the microplane. The evolution of damage on microplane level is controlled by the scalar damage value ϕ which is defined as follows

$$\phi = \begin{cases} 1 & \text{if } e_{\max} \leq e_{\mathrm{p}} \\ \sqrt{\frac{e_{\mathrm{p}}}{e_{\max}} \exp(-\frac{e_{\max}-e_{\mathrm{p}}}{e_{\mathrm{f}}-e_{\mathrm{p}}})} & \text{if } e_{\max} \geq e_{\mathrm{p}}. \end{cases} \tag{6}$$

The material parameters e_{p} and e_{f} are controlling the elastic limit and the ductility, respectively. $e_{\max}$ is the maximal equivalent microplane strain in loading history. The equivalent microplane strain e is a scalar that is defined using the normal and tangential part of the microplane strain vector as follows

$$e = \sqrt{\langle e_{\mathrm{N}} \rangle^2 + c\, \boldsymbol{e}_{\mathrm{T}} \cdot \boldsymbol{e}_{\mathrm{T}}} \tag{7}$$

where c is a non-negative parameter. The normal-tangential split (N-T split) of the microplane strain vector is performed as follows

$$e_{\mathrm{N}} = \boldsymbol{n} \cdot \boldsymbol{e} \tag{8}$$

$$\boldsymbol{e}_{\mathrm{T}} = \boldsymbol{e} - e_{\mathrm{N}} \boldsymbol{n} \tag{9}$$

where $\boldsymbol{e} = \boldsymbol{\varepsilon} \cdot \boldsymbol{n}$ is the strain vector on each microplane, calculated using the projection of the strain tensor $\boldsymbol{\varepsilon}$. With this microplane damage model it is assumed that crack initiation is mainly caused by tension. Furthermore, only small strains are considered.

As it is well-known, when modeling plain concrete using this kind of microplane damage model, mesh sensitivity is observed. This means that the strain softening behavior varies depending on the chosen mesh. Thus, a regularization of the model is necessary. There exist different approaches for this problem, including the crack band method, see [4], the integral-type nonlocal formulation, see e.g. [5] and the implicit gradient models, see e.g. [6]. In this case, the crack band model is chosen to regularize the microplane damage model, since it does not require any additional unknowns and is easy to implement. The main goal of the crack band model is to have the same energy dissipated regardless of the mesh size. This is achieved here by adjusting the two material parameters e_{p} and e_{f} with respect to the equivalent element size L_e as follows

$$e_{\mathrm{p}} = \frac{f_{\mathrm{ct}}}{E(1-m^2)} \left(1.95 - \frac{0.95}{\sqrt{\gamma - 1}}\right)^{-1} \tag{10}$$

$$e_{\mathrm{f}} = \frac{\frac{G_{\mathrm{f}}}{(1-m)L^e E e_{\mathrm{p}}} + (2.13 - 1.13m)e_{\mathrm{p}}}{2.73 - m}, \tag{11}$$

see Sharei [7]. f_{ct} denotes the tensile strength of the concrete, G_{f} is the fracture energy and m is a material parameter for compression. The parameter γ is defined as

$$\gamma = \frac{E\, G_{\mathrm{f}}}{L^e\, f_{\mathrm{ct}}^2}. \tag{12}$$

Since SBIGA does not include standard shaped elements but trapezoidal prisms and pyramid-shaped elements of different sizes, special focus was placed on the choice of the equivalent element size L^e. In a first attempt, the equivalent element size is chosen so that it depends on the volume of each element, i.e.

$$L^e = \sqrt[3]{V_e}. \tag{13}$$

This way, the different shapes and sizes of the elements in the scaled boundary representation method are automatically taken into account.

3 Numerical examples

3.1 Tensile test for plain concrete

In the first example, the microplane damage model in combination with the scaled boundary isogeometric analysis is tested for plain concrete, where the regularization of the method is necessary. As described in Sec. 2 this is done using the crack band method with the equivalent element size depending on the volume of each element. A cube with dimensions $100 \times 100 \times 100$ is subjected to uniaxial tension. Three different meshes are considered, $1 \times 1 \times 1$, $2 \times 2 \times 2$ and $3 \times 3 \times 3$ elements per direction as shown in Fig. 3, where in the scaled boundary method when saying directions we refer to the scaling direction and the two directions of the boundary surfaces. The polynomial degree for each direction was chosen to be $p = q = r = 1$. The stress-strain diagrams for the case where no regularization was applied and the case where the crack band method was applied are depicted in Figs. 4 and 5. As expected, when no regularization is used, a strong mesh dependency is observed, i.e.

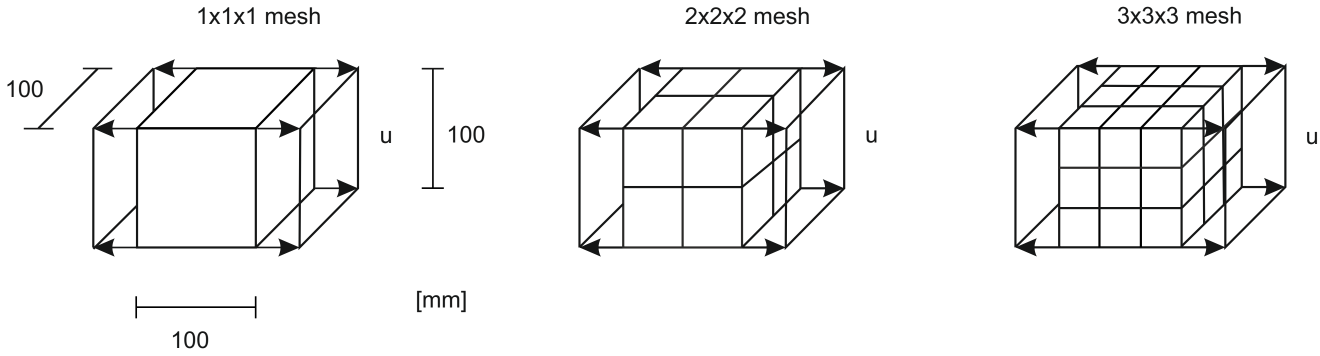

Fig. 3: The three different meshes for the tensile test of plain concrete.

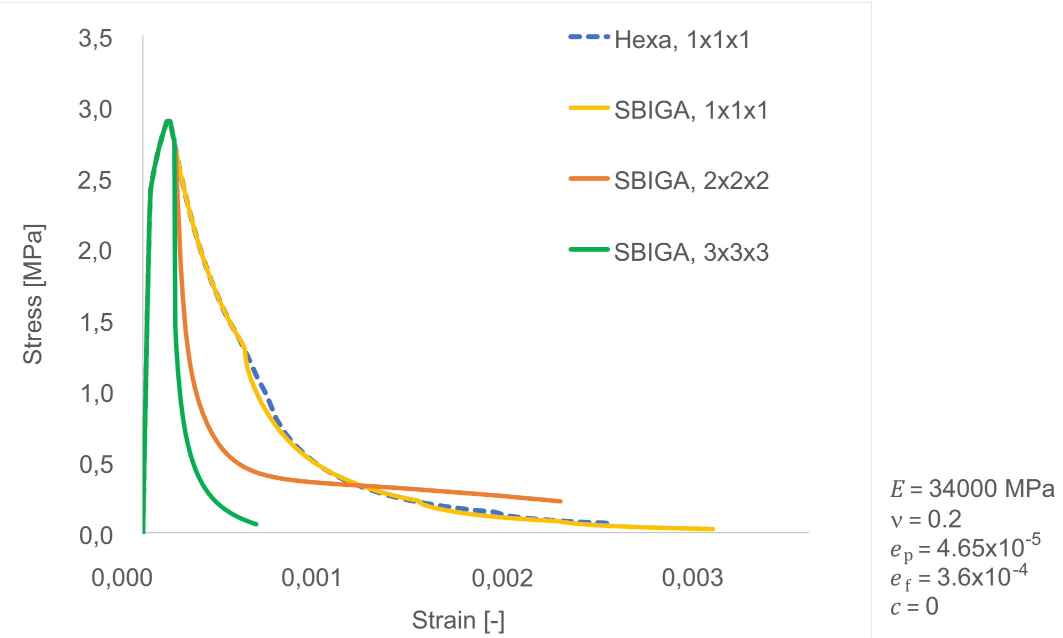

Fig. 4: Tensile test of plain concrete modeled using three different meshes. No regularization method was applied.

the post-peak behavior strongly varies depending on the mesh that was chosen. On the other hand, when applying the crack band method, the results are improved and the stress-strain curves lie close to each other. However, some small differences are still visible and compared to the results of a standard 8-node brick element with a $1 \times 1 \times 1$ mesh, the stresses have been slightly overestimated. This is an indication that the equivalent element size that was chosen was too large and should be further adjusted.

3.2 Tensile test of carbon reinforced concrete

In the second example, a carbon reinforced concrete cube is considered. It is clamped at one edge and on the opposite edge displacement-controlled loading is applied. The geometry and loading, as well as the carbon rovings inside of the concrete cube are depicted in Fig. 6. The rovings are assumed to have elliptical shape. The material parameters for the concrete are: $E_{\mathrm{con}} = 33000$ MPa and $\nu = 0.2$. The parameters for the microplane damage model where chosen as $e_{\mathrm{p}} = 4.65 \times 10^{-5}$, $e_{\mathrm{f}} = 3.6 \times 10^{-4}$ and $c = 0$. The carbon rovings are modeled only as linear-elastic material with $E_{\mathrm{carb}} = 142000$ MPa and $\nu = 0.35$. Shape functions with polynomial degree $p = q = r = 3$ were chosen for the description of the concrete and the carbon roving geometries. One goal of this research project is to apply the microplane damage model to the multiscale model of [8], where the SRVE (Shell Representative Volume Element) is modeled with SBIGA. The chosen structure in this example looks like a typical SRVE that would be used to describe a carbon reinforced concrete shell structure. Three different meshes were used for the carbon reinforced concrete cube as shown in Fig. 7. In Fig. 8 the force-displacement curve is depicted for the three different meshes. As can be seen, for all three cases the results are exactly the same. The strain hardening behavior, which occurs due to the reinforcement of the concrete, has also been reproduced.

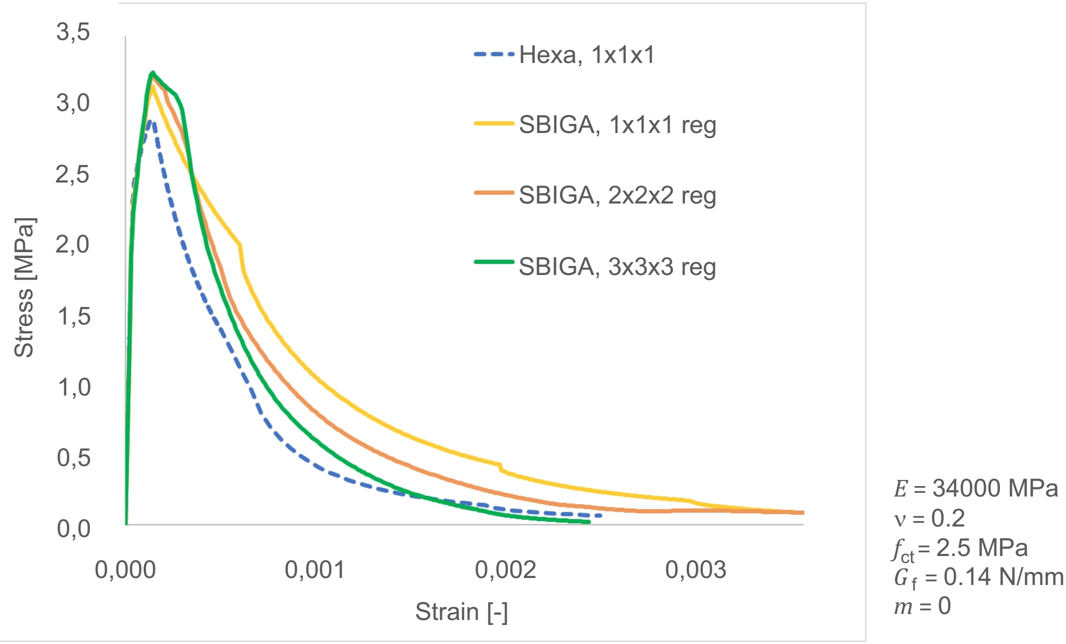

Fig. 5: Tensile test of plain concrete modeled using three different meshes. The crack band method was applied.

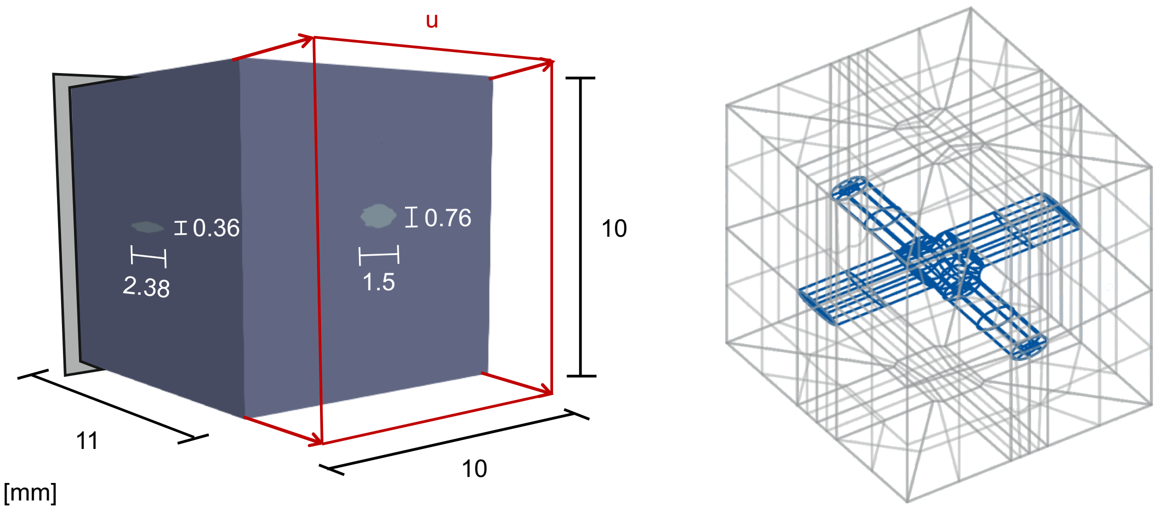

Fig. 6: Carbon reinforced concrete cube subjected to tension. On the right the geometry and position of the embedded carbon rovings are depicted.

4 Conclusions

In this work, a microplane damage model was tested in combination with the scaled boundary isogeometric analysis. The crack band method was used in order to avoid mesh sensitivity when considering plain concrete. The method was adjusted to the special element geometries that occur in the scaled boundary representation. In a first example, the tensile test of a plain concrete cube was considered in order to verify the chosen regularization technique. The results were improved compared to the case were no regularization method was applied. In a second step, the tensile test of a carbon reinforced concrete cube was examined. The strain hardening behavior was reproduced and the same results were achieved regardless of the chosen mesh. In the future, the application of the microplane damage model to the multiscale model of [8], where the scaled boundary isogeometric analysis is used on RVE-level, is planned. Regarding the regularization of the microplane damage model, further improvement of the results could be achieved by adjusting the equivalent element size. Furthermore, the calibration of the model in order to verify it using experimental data is one of the future goals.

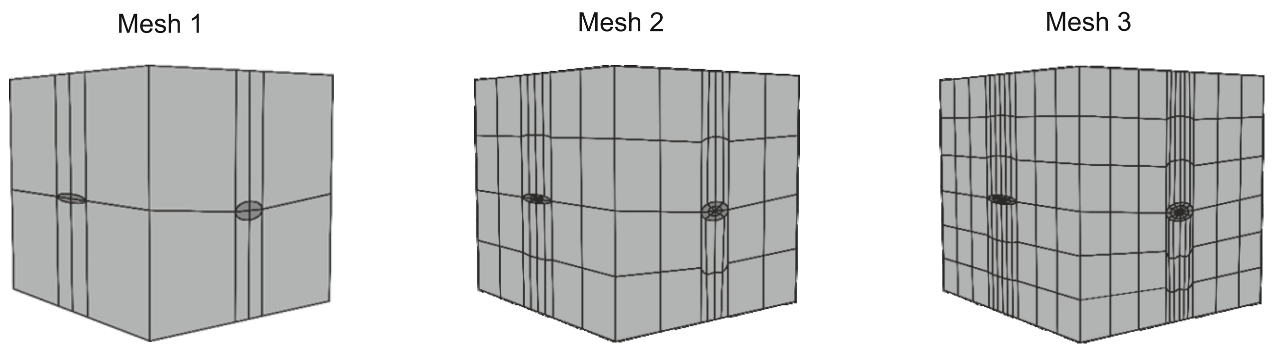

Fig. 7: Three different meshes for the carbon reinforced concrete cube.

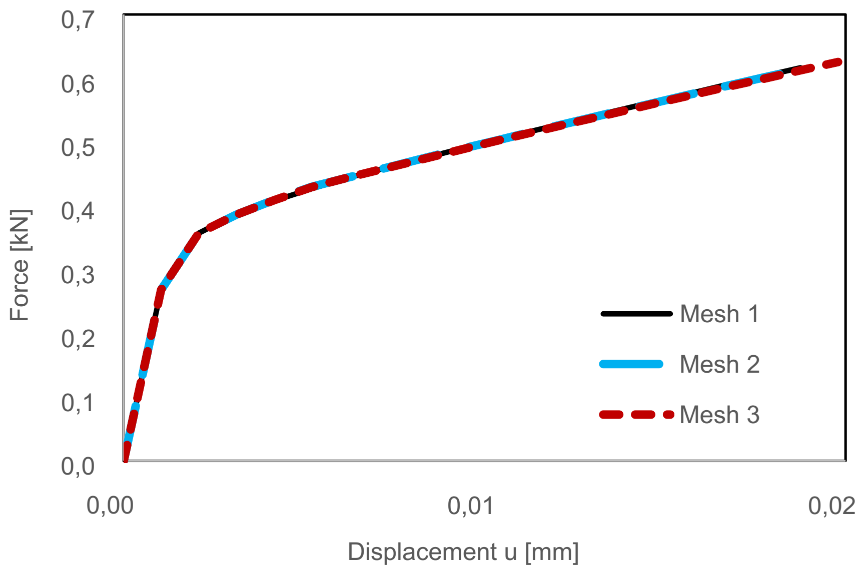

Fig. 8: Force-displacement curve of the carbon reinforced concrete using three different meshes.

Acknowledgements Open access funding enabled and organized by Projekt DEAL.

References

[1] M. Chasapi, L. Mester, B. Simeon, S. Klinkel, Int. J. Numer. Methods Eng. **123**, 1228-1252 (2021).
[2] M. Jirásek, Hermes Science Publications Paris, 55-77 (1999).
[3] R. Chudoba, E. Sharei, and A. Scholzen, Compos. Struct. **152**, 913-928 (2016).
[4] Z. Bažant, B.H. Oh, Matériaux et Construction, **16**, 155-177 (1983).
[5] G. Borino, B. Failla, F. Parrinello, Int. J. Solids Struct., **40**, 3621-3645 (2003).
[6] I. Zreid, M. Kaliske, Comput. Mech. **62**, 1239-1257 (2018).
[7] E. Sharei, Dissertation, RWTH Aachen University, Aachen (2018).
[8] L. Mester, S. Klarmann, and S. Klinkel, Proc. Appl. Math. Mech. **21**, e202100157 (2021).